BIOCHEMISTRY
including biophysical chemistry & molecular biology

Article

pubs.acs.org/biochemistry

Crystal Structure of the Marburg Virus GP2 Core Domain in Its Postfusion Conformation

Jayne F. Koellhoffer,[†] Vladimir N. Malashkevich,[†] Joseph S. Harrison,[†] Rafael Toro,[†] Rahul C. Bhosle,[†] Kartik Chandran,[‡] Steven C. Almo,[†] and Jonathan R. Lai*[,†]

[†]Department of Biochemistry and [‡]Department of Microbiology and Immunology, Albert Einstein College of Medicine, 1300 Morris Park Avenue, Bronx, New York 10461, United States

Supporting Information

ABSTRACT: Marburg virus (MARV) and Ebola virus (EBOV) are members of the family *Filoviridae* ("filoviruses") and cause severe hemorrhagic fever with human case fatality rates of up to 90%. Filovirus infection requires fusion of the host cell and virus membranes, a process that is mediated by the envelope glycoprotein (GP). GP contains two subunits, the surface subunit (GP1), which is responsible for cell attachment, and the transmembrane subunit (GP2), which catalyzes membrane fusion. The GP2 ectodomain contains two heptad repeat regions, N-terminal and C-terminal (NHR and CHR, respectively), that adopt a six-helix bundle during the fusion process. The refolding of this six-helix bundle provides the thermodynamic driving force to overcome barriers associated with membrane fusion. Here we report the crystal structure of the MARV GP2 core domain in its postfusion (six-helix bundle) conformation at 1.9 Å resolution. The MARV GP2 core domain backbone conformation is virtually identical to that of EBOV GP2 (reported previously), and consists of a central NHR core trimeric coiled coil packed against peripheral CHR α-helices and an intervening loop and helix−turn−helix segments. We previously reported that the stability of the MARV GP2 postfusion structure is highly pH-dependent, with increasing stability at lower pH [Harrison, J. S., Koellhoffer, J. K., Chandran, K., and Lai, J. R. (2012) *Biochemistry 51*, 2515−2525]. We hypothesized that this pH-dependent stability provides a mechanism for conformational control such that the postfusion six-helix bundle is promoted in the environments of appropriately mature endosomes. In this report, a structural rationale for this pH-dependent stability is described and involves a high-density array of core and surface acidic side chains at the midsection of the structure, termed the "anion stripe". In addition, many surface-exposed salt bridges likely contribute to the stabilization of the postfusion structure at low pH. These results provide structural insights into the mechanism of MARV GP2-mediated membrane fusion.

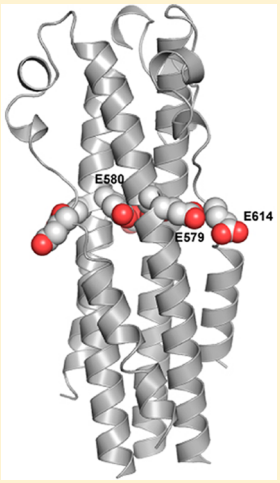

Marburg virus (MARV) and Ebola virus (EBOV) constitute the family *Filoviridae* of enveloped, negative-stranded RNA viruses ("filoviruses") that cause severe hemorrhagic fever in humans and non-human primates.[1−3] Although filovirus infections are rare, in recent years there has been an increasing frequency of outbreaks of the most pathogenic species (*Zaire* EBOV and *Sudan* EBOV), and incidences of novel species.[4] Filovirus infection is associated with high human case fatality rates (50−90% in larger outbreaks), and there are currently no Food and Drug Administration-approved therapies in the United States. For these reasons, filoviruses are classified as high-priority (Category A) biodefense pathogens by the National Institute of Allergy and Infectious Diseases and the Centers for Disease Control and Prevention.

As with other enveloped viruses, infection by MARV and EBOV requires fusion of the viral and host cell membranes, a process that is facilitated by the envelope glycoprotein GP.[5] Fusion of two lipid bilayers is an overall energetically favorable process, but there is a high kinetic barrier associated with bringing the negatively charged lipid surfaces into proximity and introducing deformations into the membranes that are required for lipid mixing.[6] In the structurally defined "class I" viral fusion proteins, this barrier is overcome by energy released from the folding of a highly stable six-helix bundle by the ectodomain of the glycoprotein.[6−9] In its prefusion form, filovirus GP is present on the viral surface as a trimeric spike consisting of three copies of the GP1−GP2 heterodimer. GP1 is the larger surface subunit, and GP2 is the smaller transmembrane subunit.[5,10] Viral entry is initiated by binding of GP1 to cell surface receptors or lectins (e.g., TIM-1 and DC-SIGN).[11−13] In EBOV entry, which has been well characterized, the virus is then taken up into the endosome where host cysteine proteases cathepsin B and cathepsin L (CatB and CatL, respectively) remove all but a 17 kDa fragment of GP1.[14−16] It is thought that host factors interact with the remaining GP1 fragment to initiate the fusion reaction. Recent work has implicated the endosomal cholesterol transporter Niemann Pick C1 (NPC1) as one receptor,[17,18] although other host factors may be required. A conformational change in GP2

Received: July 20, 2012
Revised: August 30, 2012
Published: August 30, 2012

then results in insertion of the hydrophobic fusion peptide into the host cell membrane, resulting in the "extended" or "prehairpin" intermediate. Next, two heptad repeat regions (N-terminal, NHR, and C-terminal, CHR) of the GP2 ectodomain fold into the six-helix bundle, which draws the host cell and virus membranes into proximity and promotes their coalescence.[5] It is presumed that the molecular events leading to MARV entry are similar; however, biological studies indicate that there may be some differences.[19]

Two crystal structures were reported in the late 1990s for the EBOV GP2 core domain six-helix bundle [Protein Data Bank (PDB) entry 1EBO, from Weissenhorn et al.,[20] and PDB entry 2EBO, from Malashkevich et al.[21]]. The EBOV GP2 segments of the two structures were in agreement and revealed that the core domain consists of a long, central triple-stranded core NHR α-helical trimer with the CHR α-helices and intervening loop and helix−turn−helix segments packed in an antiparallel configuration about the periphery. Here we report the crystal structure of the MARV GP2 core domain fused to a trimeric GCN4 variant at 1.9 Å resolution. The backbone conformation of the MARV GP2 core domain is essentially identical to that of EBOV GP2.

It has been well established that the conformation and/or structural stability of the envelope glycoproteins from many viruses that enter through the endocytic pathway changes upon exposure to acidic pH. A classic example is that of the influenza A virus glycoprotein, HA, where acidic pH destabilizes the interactions between HA1 (the surface subunit) and HA2 (the transmembrane subunit) and promotes projection of the HA2 fusion peptide into the host cell membrane.[22] This destabilization decreases the energetic barrier between the prefusion and postfusion conformations, facilitating formation of the postfusion HA2 conformation.[22,23] Another example is the alphavirus Semliki Forest Virus (SFV), which enters cells through a low-pH-induced conformational change in its envelope glycoproteins E1 and E2 (these glycoproteins belong to the "class II" category that contain a high β-sheet content). Upon exposure to acidic pH, protonation of histidine residues in the E1−E2 core is thought to cause dissociation of E1 and E2 and lead to the E2 postfusion conformation.[24,25] This type of pH-mediated entry occurs in other class II viruses as well, including many alphaviruses and flaviviruses.[26,27]

Portions of filovirus GP also exhibit pH-dependent structural effects. The fusion loop of EBOV GP has membrane lytic activity but only at acidic pH.[28] Recent work in our lab has demonstrated that the postfusion conformations of EBOV and MARV GP are stabilized at acidic pH.[29,30] Synthetic proteins that mimic the postfusion α-helical bundle of EBOV GP2 were more stable to thermal denaturation at acidic pH.[29] Mutational analysis suggested that interactions among acidic residues (e.g., E564, D621, D624, and D629) are important for this pH-dependent stability.[29] We noted a similar phenomemon for the postfusion structure of MARV GP2.[30] On the basis of the MARV GP2 crystal structure reported here, and site-directed mutagenesis data, we propose that an "anion stripe" across the midsection of the postfusion structure involving the core NHR residue E580 and peripheral residues E579 and E614 accounts for this pH-dependent stability. In the context of viral entry, these pH-dependent effects presumably function as a method of conformational control such that the postfusion conformation is most favored under conditions of the appropriate cellular compartment. Together, these results suggest that a combination of acidic pH-dependent structural changes in GP and the presence of endosomal resident proteins (cysteine proteases and NPC1) are required for triggering filovirus membrane fusion.

MATERIALS AND METHODS

Protein Expression and Purification. Synthetic DNA fragments encoding "pII-MarV_{IF}" and "pII-MarV_{OOF}" (see Results) were obtained from a commercial supplier (Genewiz, South Plainfield, NJ). The genes were cloned into pET22b vectors (Novagen, Madison, WI) using NdeI and XhoI restriction sites, resulting in expression plasmids pJFK1 and pJFK2, respectively. Similar methods were used for expression, purification, and refolding of both constructs. pJFK1 or pJFK2 was introduced into chemically competent *Escherichia coli* BL21 DE3 cells (Invitrogen, Carlsbad, CA) by heat shock at 42 °C. These cells were grown in LB broth at 37 °C to an OD_{600} of ∼0.6, at which point protein expression was induced by the addition of 1 mM isopropyl β-D-1-thiogalactopyranoside (IPTG). The culture was incubated at 37 °C while being shaken at 220 rpm for an additional 14−18 h. The cells were harvested by centrifugation and lysed by being stirred in 6 M guanidine hydrochloride (GdnHCl) for 2 h at room temperature. The cell debris was removed by ultracentrifugation, and the supernatant was incubated with Ni-NTA resin (Qiagen, Valencia, CA) for 1 h at room temperature. The resin was washed with 10 column volumes of 6 M GdnHCl in phosphate-buffered saline (PBS) containing 50 mM imidazole. The proteins pII-MarV_{IF} and pII-MarV_{OOF} were eluted with 6 M GdnHCl in PBS containing 250 mM imidazole. A second purification step was performed on the eluted protein, by reverse phase high-performance liquid chromatography (RP-HPLC) on a Vydac (Hesperia, CA) C18 column (10 μM, 250 mm × 21.2 mm) with water/trifluoroacetic acid and acetonitrile mobile phases. The collected pure protein fractions were combined and lyophilized and then redissolved in 5−10 mL of 6 M GdnHCl in PBS. The proteins were refolded by stepwise dialysis first into 100 mM glycine (pH 3.5) with 2 mM tris(2-carboxyethyl)phosphine (TCEP) for ∼6 h, followed by dialysis into 10 mM sodium acetate (pH 5.3, ∼14 h). Expression and purification of MarVGP2-S were conducted as previously described.[30]

Circular Dichroism (CD) Spectroscopy. Measurements were performed on a Jasco J-815 spectrometer with a 1 cm quartz cuvette for the thermal denaturation experiments and a 0.1 cm quartz cuvette for the chemical denaturation experiments. Protein concentrations for CD ranged from 0.5 to 1.5 μM, as determined by the absorbance at 280 nm. Full-wavelength scans were obtained with a 1 nm step size and a 2 s averaging time. The signal was converted to mean molar ellipticity (θ) using the equation θ (in deg cm^2 dmol^{-1}) = (millidegrees × mean residue weight)/(path length in millimeters × protein concentration in milligrams per milliliter), where the mean residue weight is the molecular weight divided by the number of backbone amides.

Thermal and chemical denaturation was monitored at 222 nm (θ_{222}). For thermal denaturation, protein samples were added to the appropriate buffer [either 10 mM sodium acetate (pH 5.3) or 20 mM sodium phosphate (pH 7.0)] in a 1 cm path length quartz cuvette and equilibrated for 1 min before measurements were taken at 15 °C. The sample was stirred constantly as the temperature was increased, and data points were collected every 3−5 °C after equilibration for ∼2 min at each temperature. θ_{222} was plotted as a function of temperature

and converted to fraction unfolded (F_{UNF}) using the equation $F_{UNF} = (\theta_{222} - \theta_{UNF})/(\theta_{FOL} - \theta_{UNF})$, where θ_{UNF} and θ_{FOL} are the CD signals for the unfolded and folded states, respectively. The F_{UNF} versus temperature data were fit to a standard four-parameter logistic equation using Graphpad Prism (GraphPad Software, La Jolla, CA); the melting temperature (T_M) was obtained from the infection point of this curve. Unmanipulated data (θ_{222} vs temperature) are shown in Figures 2 and 7. Chemical denaturation was performed by dilution of the protein samples into analysis buffers containing various GdnHCl concentrations. The solution was mixed in a 1.5 mL plastic Eppendorf tube, allowed to equilibrate for 1 min after the protein had been added, and transferred to a 0.1 cm quartz cuvette, and then θ_{222} was measured. The data were plotted as a function of GdnHCl concentration and converted to F_{UNF} as above.

X-ray Diffraction Data Collection and Crystallographic Refinement. Both pII-MarV$_{IF}$ and pII-MarV$_{OOF}$ constructs were screened for crystallization using MCSG screening kits (Microlytic, Burlington, MA) in 96-well sitting drop trays. Prior to crystallization, the proteins were concentrated to ~2.9 mg/mL in 10 mM sodium acetate (pH 5.3). Crystals for the pII-MarV$_{IF}$ construct exhibiting the best diffraction were grown in 0.17 M sodium acetate, 0.085 M Tris-HCl, 25.5% PEG3350, and 15% glycerol (pH 8.5). Crystals with overall dimensions of 0.15 mm × 0.15 mm × 0.15 mm were mounted in cryo-loops directly from the crystallization droplet and flash-cooled in liquid nitrogen. Diffraction data were collected on a Quantum 315 CCD detector (Area Detector Systems Corp., Poway, CA) with 1.075 Å wavelength radiation on beamline X29A (National Synchrotron Light Source, Brookhaven National Laboratory, Upton, NY). Intensities were integrated using HKL2000 and reduced to amplitudes using SCALEPACK2MTZ (Table 1).[31,32]

The structure of pII-MarV$_{IF}$ was determined by molecular replacement with PHASER.[33] The EBOV GP2 postfusion structure (PDB entry 2EBO) truncated to polyserine was used as a search model. Model building and refinement were performed with COOT and REFMAC.[32,34] The quality of the final structure was verified with composite omit maps. Stereochemistry was checked with MOLPROBITY.[35] LSQKAB and SSM algorithms were used for structural superpositions.[32,36] Structural figures were prepared using PyMOL (Schrödinger, LLC, New York, NY).

Limited Proteolysis. Proteases were obtained from Sigma-Aldrich (St. Louis, MO), and stock solutions were prepared as indicated in Table 2. In vitro proteolysis was performed by incubating the protein samples with each protease at either 0.1 or 0.01 mg/mL and at 37 °C for 20 min or 2 h. Reactions were quenched by the addition of 0.1 mg/mL protease inhibitor (Roche Applied Sciences, Indianapolis, IN) and placement of the samples on ice. Purification of the proteolysis products was performed immediately on a Sephadex S75 column (GE, Piscataway, NJ) in 10 mM sodium acetate (pH 5.3) with 250 mM sodium chloride at 4 °C. Protein samples were loaded at concentrations of 90−150 μM, and elution was monitored by absorbance at 280 nm. Fractions containing purified protease-stable fragments were combined and concentrated.

Mass Spectrometry Analysis. Mass spectrometry analysis of the intact and protease-stable fragments of MarVGP2-S, pII-MarV$_{IF}$, and pII-MarV$_{OOF}$ was performed on an LTQ linear ion trap mass spectrometer interfaced with a Rapid Separation LC 3000 system (Thermo Scientific, San Jose, CA).

Table 1. Data Collection and Refinement Statistics for the pII-MarV$_{IF}$ Crystal Structure

PDB entry	4G2K
Data Collection	
wavelength (Å)	1.075
space group	$P2_12_12$
unit cell dimensions	a = 52.57 Å
	b = 147.53 Å
	c = 42.20 Å
	$\alpha = \beta = \gamma = 90°$
resolution range (Å)	1.9−20.0
no. of observed reflections	260604
no. of unique reflections	26888
completeness (%)[a]	99.6 (94.3)
R_{sym}	0.071 (0.583)
$I/\sigma I$	11.5 (2.9)
R_{merge} (I)[b]	
Structure Refinement	
R_{cryst} (%)[c]	0.197
R_{free} (%)[c]	0.248
no. of protein non-hydrogen atoms	2421
no. of water molecules	249
average B factor (Å^2)	35.0
rmsd from ideal value	
bonds (Å)	0.011
angles (deg)	1.28
torsion angles (deg)	17.1

[a]Values in parentheses indicate statistics for the high-resolution bin (1.95−1.9 Å). [b]$R_{merge} = \sum_j\sum_j|I_j(hkl) - \langle I(hkl)\rangle|/\sum_j\sum_j|\langle I(hkl)\rangle|$, where I_j is the intensity measurement for reflection j and $\langle I\rangle$ is the mean intensity over j reflections. [c]R_{cryst} (R_{free}) $= \sum||F_o(hkl)| - |F_c(hkl)||/\sum|F_o(hkl)|$, where F_o and F_c are observed and calculated structure factors, respectively. No σ cutoff was applied; 5% of the reflections were excluded from refinement and used to calculate R_{free}.

Table 2. Proteases and Conditions for Limited Proteolysis

protease	Sigma-Aldrich catalog no.	buffer
α-chymotrypsin	C3142	1 mM HCl, 2 mM $CaCl_2$
trypsin	T8003	1 mM HCl, 2 mM $CaCl_2$
elastase	E0127	200 mM Tris-HCl
papain	P5306	H_2O
proteinase K	P2308	4 mM $CaCl_2$

For MS/MS sequencing, the protein samples were reduced with 10 mM TCEP and alkylated with 55 mM iodoacetamide, both in 25 mM ammonium bicarbonate (pH 8.0). The samples were then digested overnight at 37 °C in a 50 mM ammonium bicarbonate solution (pH 8.0) using L-1-tosylamido-2-phenylethyl chloromethyl ketone (TPCK)-modified trypsin immobilized on beads (Thermo Scientific, San Jose, CA). The resulting tryptic peptides were desalted using C18 Zip Tip with a 0.6 μL microbed volume (Millipore, Billerica, MA) and diluted with a 2% acetonitrile/2% trifluoroacetic acid mixture to 45 μL for mass spectrometry analysis.

Nanospray liquid chromatography and mass spectrometry were performed on an LTQ linear ion trap mass spectrometer interfaced with a Rapid Separation LC 3000 system (Thermo Scientific); 40 μL of sample was loaded onto an Acclaim PepMap C18 Nanotrap column (5 mm, 100 Å, 100 mm inside diameter × 2 cm) in 2% acetonitrile with 0.1% trifluoroacetic acid at a flow rate of 8 μL/min. After 15 min, the trap column was switched in line with the Acclaim PepMap RSLC C18

dx.doi.org/10.1021/bi300976m | Biochemistry 2012, 51, 7665−7675

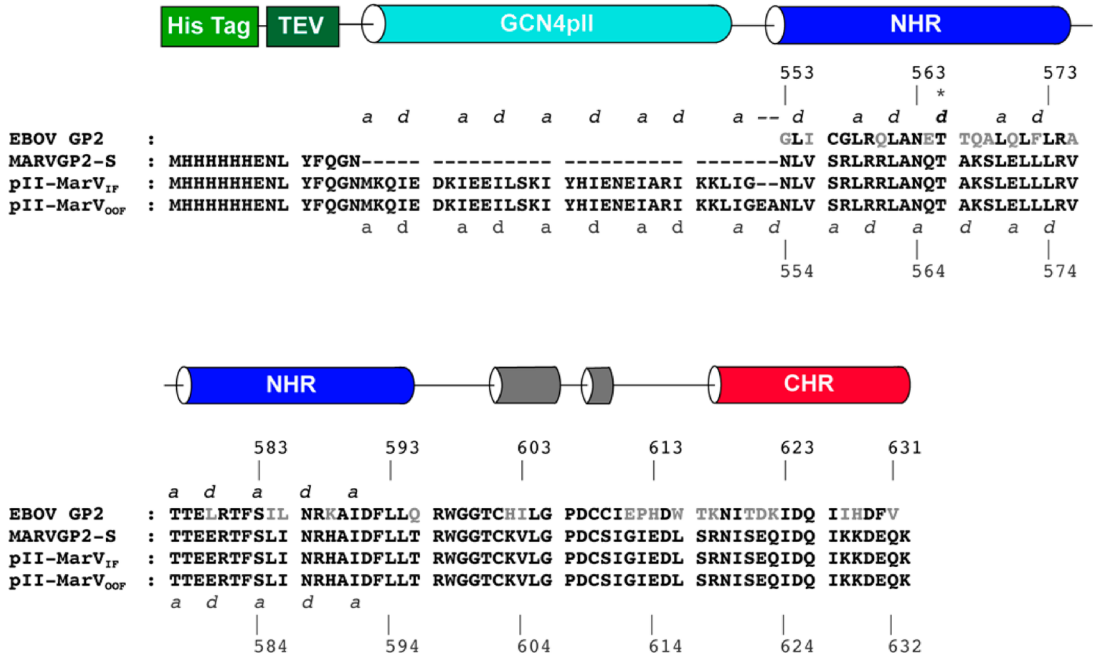

Figure 1. Protein design. The sequences of the EBOV GP2 ectodomain and the three constructs described here (MarVGP-S, pII-MarV$_{IF}$, and pII-MarV$_{OOF}$) are shown. Residues in EBOV GP2 that differ from those in MARV are colored gray. Segments corresponding to secondary structural elements for the previously reported EBOV GP2 structures, and for the pII-MarV$_{IF}$ structure, are depicted as cylinders. The colors of the cylinders match the structural elements depicted in Figure 2A for pII-MarV$_{IF}$. The amino acid numbering for EBOV and MARV GP2 differs by one; the EBOV numbering is shown above the sequences, and the MARV numbering is shown below. The ***a*** and ***d*** positions are indicated for the NHR (including the stutter at position T566, asterisk) and the GCN4 pII segment. In pII-MarV$_{IF}$, the GCN4 pII heptad repeat flows contiguously to the N-terminal end of the NHR (***a***/***d*** pattern shown below the alignment); in pII-MarV$_{OOF}$ (which differs by a two-residue insertion), the periodicity of the heptad repeat is disrupted between the GCN4 pII segment and the N-terminal end of the stutter (***a***/***d*** pattern shown above the alignment).

nanocolumn (2 μm, 100 Å, 75 μm inside diameter × 25 cm). The peptides were separated and eluted into the mass spectrometer using an acetonitrile gradient of ~1% B/min (mobile phase A = 2% acetonitrile with 0.1% formic acid; mobile phase B = 80% acetonitrile with 0.1% formic acid) at a flow rate of 300 mL/min.

The 10 most intense ions with charge states from +2 to +4 were selected for fragmentation (MS/MS). MS/MS was performed using an isolation width of m/z 2, a normalized collision energy of 35%, an activation time of 30 ms, a minimal signal intensity of 10000 counts, and the dynamic exclusion option enabled. Once an ion was selected twice for MS/MS within 15 s, it was excluded from being selected again for a duration of 60 s. The MS/MS data were submitted for Sequest search against the protein sequence through Proteome Discoverer 1.2 (Thermo Scientific) with the following search parameters: static modification Carbamidomethylation (C), dynamic modifications Deamidation (N, Q) and Oxidation (M), precursor mass tolerance of 2 Da, fragment mass tolerance of 0.6 Da, and minimal peak count of 10.

RESULTS

Protein Design. We previously characterized a protein consisting of residues 553−633 from the MARV GP2 core domain containing two Cys → Ser mutations at positions 557 and 610 (MarVGP2-S).[30] This protein adopts a stable, trimeric α-helical bundle, similar to the corresponding segment from EBOV GP2. While we were able to perform basic biophysical characterization of MarVGP2-S, it had limited solubility (<0.5 mg/mL) and expression yields were suboptimal (~0.1 mg/L of culture). To improve these properties, we prepared two MarVGP2-S variants containing N-terminal fusions to a trimeric coiled coil ("GCN4 pII"). The natural GCN4 sequence forms a dimeric coiled coil and contains the canonical heptad repeat pattern denoted ***abcdefg***, with predominantly hydrophobic residues (Leu and Val) occupying the ***a*** and ***d*** positions. A variant of GCN4 ("pII") that contains isoleucine at all ***a*** and ***d*** positions forms a stable trimeric α-helical bundle.[37] Weissenhorn et al. produced a chimeric protein consisting of the EBOV GP2 core domain with a fusion to GCN4 pII [EBOV pIIGP2(552−650), PDB entry 1EBO] at the N-terminus to promote solubility and crystallization.[20] The GCN4 pII segment has been appended to trimeric envelope glycoproteins from other viruses to enhance stability in those systems as well.[38−41]

The crystal structure of EBOV pIIGP2(552−650) revealed that the registry of the heptad repeats from GCN4 pII was out of frame with the heptad repeats of EBOV GP2.[20] The cause of this misalignment is a "stutter" in the periodicity of the EBOV GP2 postfusion conformation, near the N-terminal region of the protein at T565. α-Helices that participate in coiled coils typically contain a heptad repeat pattern displaying a 3-4-3-4 periodicity of hydrophobic residues (***abcdefg abcdefg***), where positions ***a*** and ***d*** are hydrophobic. The stutter causes an interruption of this periodicity resulting in an atypical 3-4-4-3 hydrophobic pattern (***abcdefg defgabc***). As a consequence, there is a slight distortion of the EBOV GP2 α-helices in the stutter region, and the registry of the heptad repeat is altered at the N-terminal segment of the NHR. Sequence alignment of the EBOV and MARV GP2 suggests that this stutter also exists in MARV GP2 (at T566 of MARV). Similar stutters are found in the analogous portion of the structurally related arenavirus GP2

dx.doi.org/10.1021/bi300976m | *Biochemistry* 2012, 51, 7665−7675

postfusion conformation, the flexible segment of the influenza HA2 coiled coil, and others.[23,42] We designed two chimeric constructs of MARV GP2 fused to GCN4 pII, one in which the periodicity of the GCN4 pII segments aligns with the predicted stutter ("In Frame", pII-MarV$_{IF}$) and one analogous to EBOV pIIGP2(552−650) of Weissenhorn et al. that does not account for the stutter ("Out of Frame", pII-MarV$_{OOF}$) (Figure 1). All constructs contained an N-terminal hexahistidine tag followed by the tobacco etch virus (TEV) protease substrate sequence (~ENLYFQG~).

Both pII-MarV$_{IF}$ and pII-MarV$_{OOF}$ were expressed in *E. coli*, purified from the insoluble fraction, and refolded by stepwise dialysis. As anticipated, both proteins had enhanced properties in terms of solubility (~3 mg/mL) and expression yields (>1 mg/L of culture) relative to those of MarVGP2-S.

Characterization of pII-MarV$_{IF}$ and pII-MarV$_{OOF}$. Circular dichroism indicates that both pII-MarV$_{IF}$ and pII-MarV$_{OOF}$ are α-helical, with double minima at 208 and 222 nm, in both 10 mM sodium acetate (pH 5.3) and 20 mM sodium phosphate (pH 7.0) (Figure 2A). The relative intensities of the 208 and 222 nm peaks varied with pH for both proteins, indicating that there are differences in the quaternary packing of the α-helical segments under different buffering conditions. We previously reported similar pH-dependent effects in MarVGP2-S.[30] Furthermore, we found that the thermal stability of pII-MarV$_{IF}$ and pII-MarV$_{OOF}$ was dependent on pH, with higher stability at lower pH values (Figure 2B,C), consistent with behavior previously observed with MarVGP2-S. At pH 5.3, pII-MarV$_{IF}$ could not be completely unfolded [melting temperature (T_M) estimated to be ~98 °C based on the partial denaturation curve]. However, at pH 7.0, the T_M was 55.7 ± 0.9 °C (Figure 2B). Similar pH effects were observed in pII-MarV$_{OOF}$ (Figure 2C): the T_M at pH 7.0 was 47.6 ± 0.5 °C; at pH 5.3, the denaturation curve was right-shifted but the denaturation profile was biphasic. One possible interpretation of this biphasic denaturation profile is that the break in the heptad repeat registry between the GCN4 pII segment and the MARV GP2 segment caused by the hydrophobic stutter results in noncooperative unfolding of these two distinct segments in pII-MarV$_{OOF}$. This noncooperative behavior is observed under conditions where both elements are stable (lower pH) but is masked at higher pH where the MARV GP2 segment is less stable. This biphasic behavior was not observed in pII-MarV$_{IF}$, presumably because there is no break in the heptad repeat registry between the N-terminal segment of MARV GP2 and GCN4 pII. Therefore, pII-MarV$_{IF}$ unfolds cooperatively. Chemical denaturation at pH 5.3 and 7.0 confirmed the pH-dependent stability of pII-MarV$_{IF}$ and pII-MarV$_{OOF}$ (see the Supporting Information).

Crystal Structure of pII-MarV$_{IF}$. The crystals of pII-MarV$_{IF}$ exhibited diffraction consistent with space group $P2_12_12$ with three independent pII-MarV$_{IF}$ chains (i.e., a noncrystallographic trimer in the asymmetric unit). The structure was determined at 1.9 Å resolution (Table 1 and Figure 3) using the EBOV GP2 postfusion structure (PDB entry 2EBO) as the molecular replacement search model. To mitigate model bias from the highly homologous EBOV GP2 structure, PDB entry 2EBO was truncated to polyserine prior to molecular replacement. The initial electron density map for pII-MarV$_{IF}$ clearly showed the positions of the omitted side chains and the N-terminal GCN4 pII fusion partner. The backbone conformation of the core MARV GP2 segment (residues 550−631) is virtually identical to the EBOV GP2 postfusion

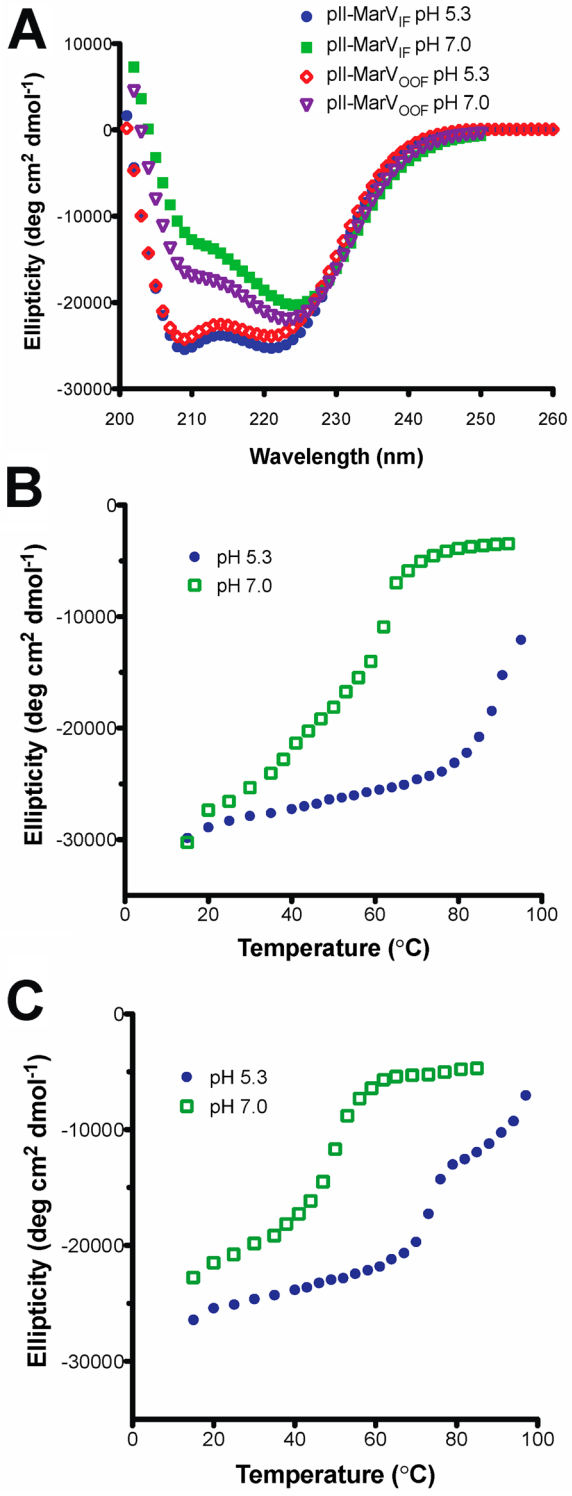

Figure 2. Analysis of pII-MarV$_{IF}$ and pII-MarV$_{OOF}$ by CD. (A) Wavelength scans of both proteins in 10 mM sodium acetate (pH 5.3) and 10 mM sodium phosphate (pH 7.0). (B and C) Thermal denaturation of pII-MarV$_{IF}$ (B) and pII-MarV$_{OOF}$ (C) at pH 5.3 and 7.0.

structure with backbone Cα rmsd values of 0.68 Å when compared to PDB entry 1EBO (residues 57−129) and 1.13 Å when compared to PDB entry 2EBO (residues 558−630) (Figure 3B). The NHR forms an elongated central trimeric coiled coil, with the polypeptide reversing direction at R597 and leading to the loop and helix−turn−helix motifs that

dx.doi.org/10.1021/bi300976m | *Biochemistry* 2012, 51, 7665−7675

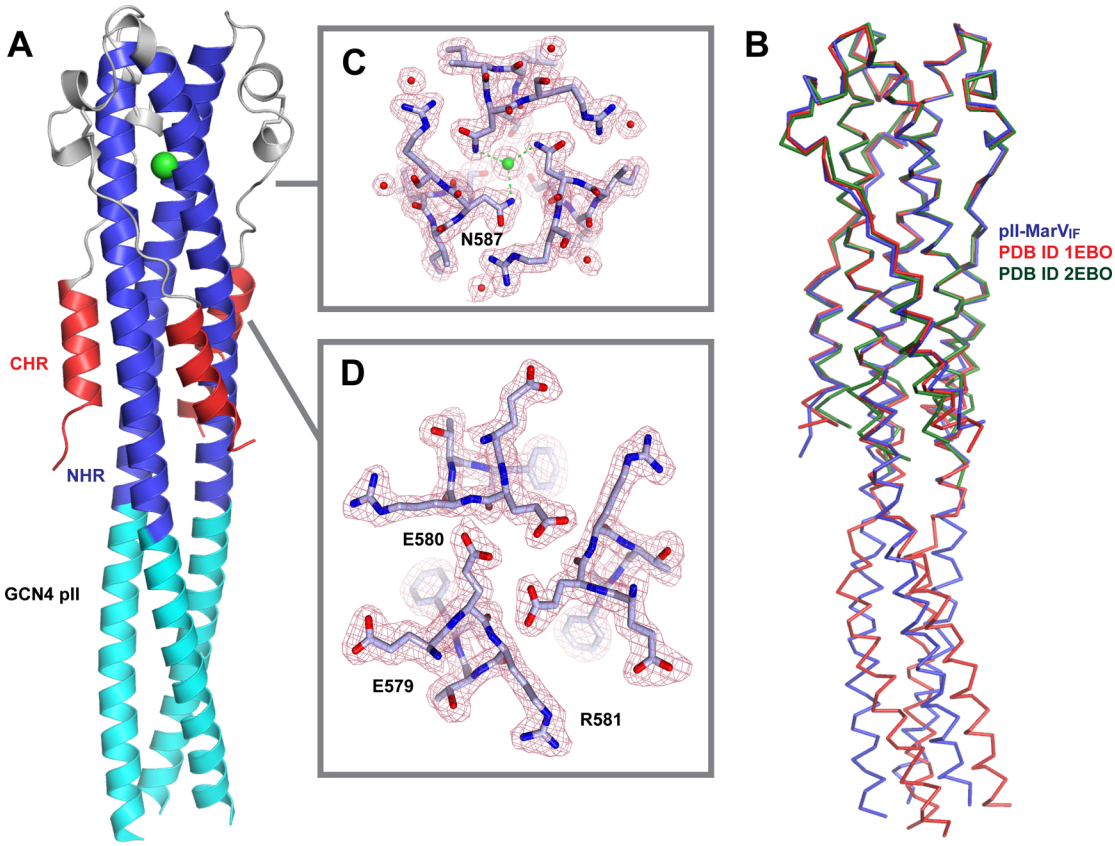

Figure 3. Structural features of the pII-MarV$_{IF}$ crystal structure. (A) Overall depiction of the fold, with secondary structural elements colored according to the cylinders in Figure 1. The chloride ion bound by N587 is shown as a green sphere and depicted with electron density in panel C. (B) Overlay of pII-MarV$_{IF}$ with the two reported EBOV GP2 structures (PDB entry 1EBO, from Weissehorn et al.,[20] and PDB entry 2EBO, from Malashkevich et al.[21]). The structural alignment was performed with the MARV/EBOV GP2 segments only. (C and D) View down the NHR trimer axis and electron density for regions near the chloride-binding site (C) and the E580 residue oriented toward the core (D).

precede the CHR. An intrachain disulfide bond between C602 and C609 stabilizes the helix−turn−helix motif, analogous to the disulfide bond between C601 and C608 in EBOV GP2. The MARV GP2 CHR α-helices are approximately three full turns in length (beginning at S617 and ending at E631) and are packed about the periphery of the NHR core trimer, distal to the turn. As predicted, the heptad repeat stutter position (T566) points toward the core, and therefore, the periodicity of the GCN4 pII segment is maintained with the N-terminal NHR segment, consistent with design. An overlay of pII-MarV$_{IF}$ and EBOV pIIGP2(552−650) demonstrates that the GCN4 pII trimer is in alignment with the core NHR trimer in pII-MarV$_{IF}$ but is distorted in EBOV pIIGP2(552−650) (Figure 3B). A chloride ion is bound in the pII-MarV$_{IF}$ core NHR trimer at N587, analogous to the anion-binding pocket observed in both EBOV GP2 structures (Figure 3C).

We previously performed site-directed mutagenesis on the MARV GP2 core domain in an attempt to identify residues in the MARV GP2 core that contributed to pH-dependent stability.[30] On the basis of homology to EBOV GP2, we predicted that MARV GP2 E580, which occupies a ***d*** position, would point toward the core. However, mutation of this residue to its neutral analogue (Gln) had no impact on pH-dependent stability. The structure of pII-MarV$_{IF}$ demonstrates that in fact this side chain is oriented toward the core of the NHR trimer (Figure 3D). Polar residues at core ***a*** or ***d*** positions are common in coiled coils and specify both α-helix orientation and registry because there is a strong driving force for pairing the polar residues from opposing α-helices in the context of a hydrophobic core.[42−45] Furthermore, anionic residues at these positions, and peripheral ***e*** and ***g*** positions, can mediate pH-dependent behavior or heterooligomerization.[46−48] While the three E580 side chains from associated NHR chains point toward the core, the polar residues do not appear to be stabilized by adjacent cationic residues or counterions. Electron density in this region is well-defined and supports the modeled side chain orientation (i.e., toward the core). It is therefore likely the E580 side chain carboxylic acid has an elevated pK_a value because deprotonation of these residues in the context of the hydrophobic core would be energetically unfavorable. In fact, Glu residues at core ***a*** and ***d*** positions or at peripheral ***e*** and ***g*** positions in other coiled-coil systems typically have elevated pK_a values.[49,50]

Although an E580Q single mutant was not dramatically altered in terms of pH-dependent stability, a double mutant containing Glu → Gln mutations at position 580 and the adjacent E579 residue had enhanced stability at pH 7.0 relative to that of WT.[30] The pII-MarV$_{IF}$ crystal structure reveals that E579 side chain Oδ atoms are approximately 5 Å from the side chain Oδ atom of E614 in the loop of the adjacent monomer (Figure 4A). As a consequence of distinct local environments in the asymmetric unit, there were some nonequivalent interactions within the trimer; the interatomic distances between proximal oxygen atoms on E579 and E614 were 4.3, 4.4, or 5.2 Å in the three different GP2 monomers. The proximity of E579 and E614 results in considerable negative

dx.doi.org/10.1021/bi300976m | *Biochemistry* 2012, 51, 7665−7675

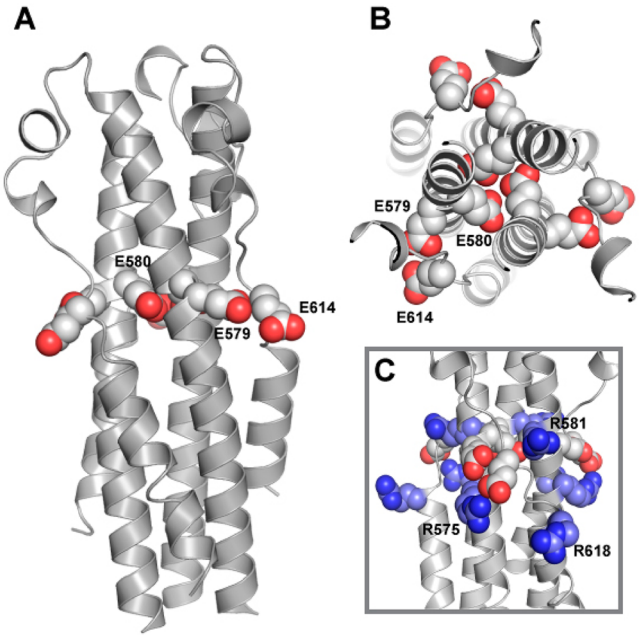

Figure 4. Anion stripe and shielding arginine residues. (A) Side chains of E579, E580, and E614 shown in a space-filling representation. (B) View of side chains that comprise the anion stripe down the NHR trimer axis. (C) Stabilizing interactions with R581, R575, and R618 (colored blue).

electrostatic surface potential near the midsection of the molecule (Figure 5). Together, E579, E580, and E614 form an anion stripe that runs across the center of the postfusion

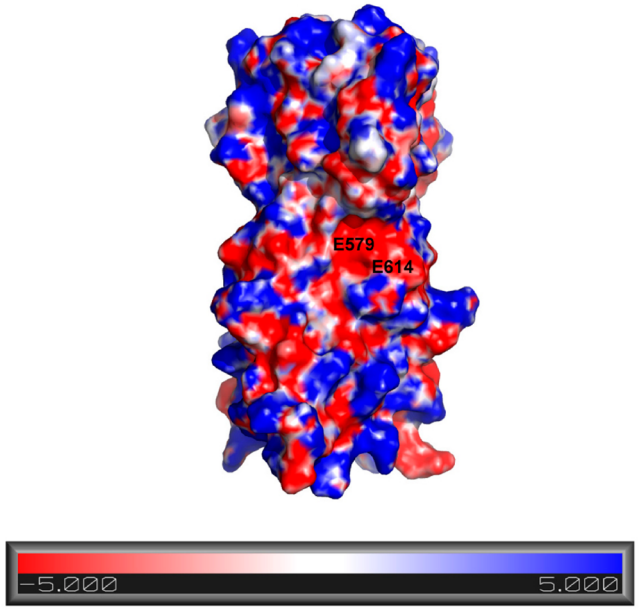

Figure 5. Calculated electrostatic surface potential. To generate the surface electrostatic map of MARV GP2, the PBEQ-Solver server was used with the generic presets (refs 62−64). A solvent accessible surface representation of MARV GP2 is shown with an electrostatic potential map (+5 kcal/mol of *e* in blue to −5 kcal/mol of *e* in red). The surface of MARV GP2 is highly charged, and the anionic stripe forms an electronegative pocket in the center of the protein. The surface-exposed residues that make up the anionic stripe, E579 and E614, are labeled.

structure (Figure 4B). We propose that the concerted interactions among carboxylic acid or carboxylate atoms (depending upon protonation state) in this anion stripe contribute to the pH-dependent stability. At higher pHs, the three side chains (E579, E580, and E614) are deprotonated, which destabilizes the core structure because of repulsion between juxtaposed negatively charged atoms. This destabilization may involve specific residue−residue interactions (for example, the three E580 side chains pointed toward the NHR core) or global effects that result from a high density of anionic residues at the center of the postfusion structure. The mechanism for pH-dependent destabilization at higher pHs likely requires concerted action of residues in the anion stripe because individual mutation of E579 or E580 to neutral analogues had little effect on pH-dependent stability.[30] Other side chains may be involved in this mechanism, such as D615, which is near the anion stripe but does not appear to interact directly with any other acidic residues.

In addition, several salt bridges may stabilize the postfusion structure (Figure 6). In all three GP2 monomers, there is

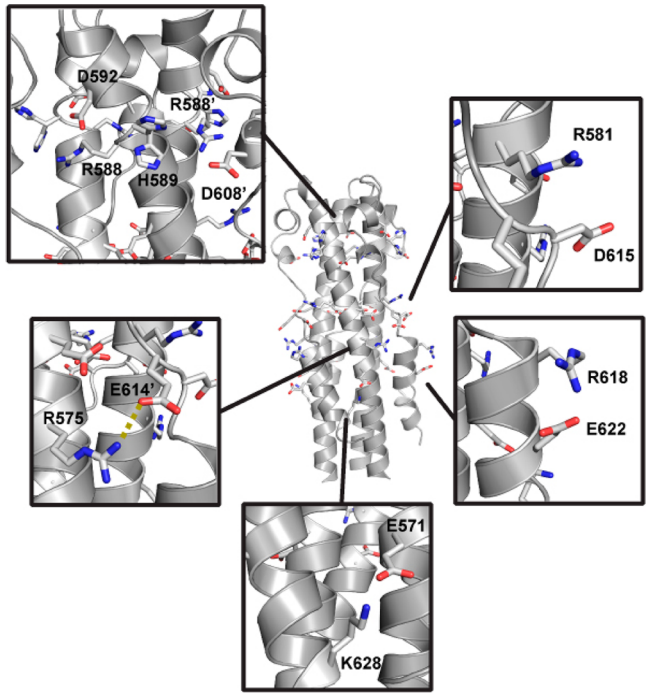

Figure 6. Salt bridges that may stabilize the postfusion conformation. For interactions involving residues from two separate monomers, the residues that are located on a different monomer are indicated with a prime symbol. Two conformations were observed for the side chain of H589.

potential for interaction between K628 Nε in the CHR and E571 Oδ in the NHR, though the electron density was not well-defined past Cγ for K628. In one of the three monomers (chain A), the side chains of R618 and E622 are oriented toward one another. In the other two monomers (chains B and C), crystal contacts from adjacent subunits or poorly defined electron density of the E622 side chain obscure this interaction, but electrostatic interactions between these two side chains are nonetheless possible in solution. In all three monomers, the terminal N atom of R575 (NHR) is <3.5 Å from E614 Oδ (loop region). The side chain of R581 is near that of D615 in all three monomers. Together, R575, R581, and R618 form two

dx.doi.org/10.1021/bi300976m | *Biochemistry* 2012, 51, 7665−7675

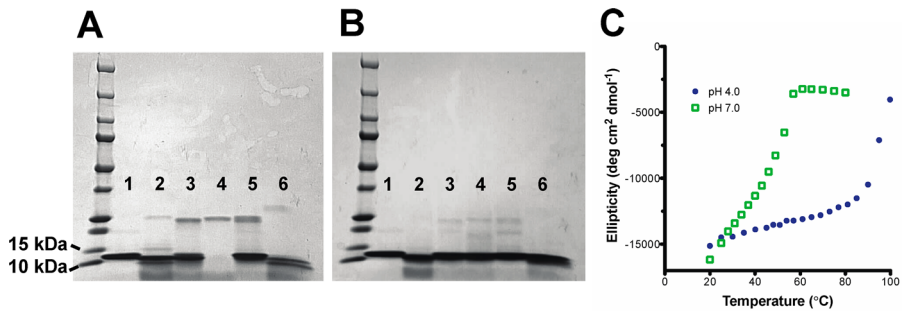

Figure 7. Limited proteolysis. Representative results for limited proteolysis of MarVGP2-S after 2 h at two protease concentrations, 0.1 (A) and 0.01 mg/mL (B): lane 1, no protease; lane 2, α-chymotrypsin; lane 3, trypsin; lane 4, elastase; lane 5, papain; lane 6, proteinase K. Complete information for proteolysis conditions can be found in Materials and Methods and Table 2. Results from similar experiments with pII-MarV_{IF} and pII-MarV_{OOF} are found in the Supporting Information, along with mass spectrometry analysis of the protease-stable fragments. (B) Thermal denaturation at pH 5.3 and 7.0 for the FPLC-purified α-chymotrypsin-stable fragment of MarVGP2-S.

layers of basic residues on the exterior of the structure that sandwiches the anion stripe (R581 above and R575 and R618 below) (Figure 4C). This configuration may serve to stabilize the high density of negative charge that could result from deprotonation of all side chains in the anion stripe. There are several additional potential salt bridges involving residues near the reverse turn. D608 could potentially participate in electrostatic interactions with R588 of the same monomer and H589 of the adjacent monomer. Similarly, a cluster of ionic residues is formed by R588, H589, and D592 within a single monomer near the end of the CHR segment.

Limited Proteolysis. To further define the stable core of MARV GP2, we subjected MarVGP2-S, pII-MarV_{IF}, and pII-MarV_{OOF} to proteolysis by a panel of common proteases: α-chymotrypsin, trypsin, elastase, papain, and proteinase K (Table 2, Figure 7A,B, and Supporting Information). Reactions were performed at two different protease concentrations (0.1 or 0.01 mg/mL), and reactions were quenched at 20 min or 2 h. These trials yielded stable fragments in all three proteins, most apparent upon cleavage with α-chymotrypsin. For all three proteins, the proteolysis with α-chymotrypsin was repeated on a large scale, and the α-chymotrypsin-stable fragment was isolated by fast performance liquid chromatography (FPLC) and characterized by mass spectrometry. For MarVGP2-S, the fragment had a molecular mass difference of −1474 Da relative to the unproteolyzed protein, which is consistent with removal of the first 11 residues comprising the hexahistidine tag and the first four residues of the engineered TEV cleavage site (removed portion had an MHHHHHHENLY~ sequence). Peptide fragmentation mass spectrometry confirmed the sequence of the protease-stable fragment (see the Supporting Information). Similarly, results of mass spectrometry analysis of the protease-stable fragments of pII-MarV_{IF} and pII-MarV_{OOF} were consistent with the conclusion that the analogous hexahistidine/TEV cleavage site was removed from those proteins as well.

It is of potential concern that the hexahistidine tag contributes to the pH-dependent stability observed in the MARV and EBOV GP2 ectodomain proteins. Generally, hexahistidine tags do not affect structural analysis, but cautionary exceptions have been noted.[51] We performed thermal denaturation of the α-chymotrypsin-stable fragment of MarVGP2-S to address these concerns, because this fragment lacks the histidine tag. We found similar pH-dependent stability (Figure 6C), demonstrating that the histidine tag plays no role in this phenomenon and that it is an intrinsic property of the native protein.

DISCUSSION

Overall, the structure of the MARV GP2 core domain suggests that interactions among ionic side chains mediate the pH-dependent stability of the postfusion conformation. On the basis of previous mutagenesis data, we propose that the anion stripe consisting of E579, E580, and E614 plays a critical role. The pH-dependent behavior may not be attributable to any single side chain−side chain interaction but rather the concerted action of the entire ensemble of acidic residues. Folding of the six-helix bundle would be most favorable under conditions where repulsive interactions between side chains in the stripe are minimized; this would be most likely at low pH when all three glutamic acid side chains are protonated. In our previous work, we reported that 500 mM NaCl stabilizes the six-helix bundle at pH 7.0 and 5.3, but that the pH-dependent stability was nonetheless observed.[30] Because the anion stripe includes residues that are surface-exposed, as well as E580, which is oriented toward the core, it seems reasonable that charge screening might have some effect on stability but would not completely abrogate the pH-dependent effects. The anion stripe does not appear to be present in EBOV GP2, as positions 580 and 614 are occupied by residues Leu and His, respectively (Figure 1). Previously, we described the pH-dependent stability of designed proteins that mimic the EBOV GP2 six-helix bundle.[29] In this case, pH-dependent stability appears to be mediated by surface-exposed interactions among acidic side chains (E564, D621, D624, and D629).

In MARV GP2, the proximity of several acidic and basic side chains suggests that a constellation of salt bridges provides further stabilization of the postfusion conformation under conditions where Glu and Asp side chains are present as carboxylate species. In general, surface-exposed salt bridges are thought to provide only minor contributions to overall stability in α-helical proteins.[52] For example, in the designed heterodimeric coiled coil known as "Acid-p1−Base-p1", all *e* and *g* positions of the two-component α-helices are occupied by either Asp (Acid-p1) or Lys (Base-p1).[46] The Acid-p1−Base-p1 heterodimer is preferred over either the Acid-p1−Acid-p1 or Base-p1−Base-p1 homodimer not because of energetic contributions from salt bridges from opposing α-helices in the heterodimer but rather because each of the homodimers is disfavored relative to the heterodimer due to repulsion.[46] At extreme pH (low pH for Acid-p1 and high pH for Base-p1), the

dx.doi.org/10.1021/bi300976m | *Biochemistry* 2012, 51, 7665−7675

homodimers are more thermostable than the heterodimer at neutral pH. However, in the context of MARV GP2, it seems plausible that the side chains of R575, R581, and R618, which form layers of cationic charges above and below the anion stripe, contribute to the overall stability by shielding the high density of anionic charges if the side chains of E579, E580, and E614 are deprotonated. This shielding effect may explain why the six-helix bundle forms at neutral pH or higher (the crystals here were grown at pH 8.5), even though it is much less stable than at lower pH. In lower-pH environments, this "shielding" of the anion stripe is less important presumably because the side chains of E579, E580, and E614 are protonated.

In solution, CD experiments suggest that there are some differences in structure at pH 7.0 and 5.3 because the ratio of 208 and 222 nm peaks differs under these conditions. However, the crystals of pII-MarV_{IF} were obtained at pH 8.5, and the core domain backbone conformation is identical to that of EBOV GP2 crystallized at pH 7.5 (PBD entry 1EBO) and pH 4.6 (PDB entry 2EBO). It is possible that inclusion of the GCN4 pII segment induces a single conformer in the crystalline state, regardless of pH, because pII-MarV_{IF} and EBOV pIIGP2(552−650) (the protein crystallized in PDB entry 1EBO) contain this segment and were crystallized at a higher pH. Because CD is inherently low resolution, it is not possible to determine if the signature represents a homogeneous conformational state or an ensemble of two or more states. However, in the context of the prefusion spike (in the presence of GP1), the EBOV GP2 NHR adopts a distinct but α-helical conformation.[10]

It is interesting to note that EBOV pIIGP2(552−650) was reported to have high thermostability (T_M > 90 °C) at pH 8.0.[20] However, we recently reported that smaller designed proteins that mimic the EBOV GP2 α-helical bundle exhibit pH-dependent stability with lower stability at neutral pH.[29] Therefore, in EBOV GP2, the length of the construct may have an effect on pH sensitivity because pIIGP2(552−650) encompasses more of the ectodomain than our designed proteins and also includes the GCN4 pII fusion. It is possible that the EBOV GP2 postfusion structure is less sensitive to pH than is the MARV GP2 postfusion structure because both pII-MarVGP2$_{OOF}$ and pII-MarVGP2$_{IF}$ were much less stable at pH 7.0 than EBOV pIIGP2(552−650) at pH 8.0. Whether these differences reflect variations in the mechanisms of EBOV and MARV entry remains to be determined.

The mechanism of pH-dependent stability for the MARV and EBOV GP2 contrasts with those of influenza HA and SFV E1 and E2. In influenza HA and SFV E1 and E2, exposure to acidic pH disrupts or destabilizes the prefusion conformation, which presumably decreases the barrier to the lowest-energy postfusion conformation.[22−27] Therefore, acidic pH plays a direct role in early fusion events by inducing structural changes in the glycoprotein. In MARV and EBOV GP2, acidic pH stabilizes (and therefore favors the formation of) the postfusion conformation.[29,30] Low pH is likely required for early steps in the fusion pathway, because CatL, CatB, and other endosomal proteases are most active at pH ∼5. These proteolysis steps are necessary but not sufficient for viral entry; exposure to low pH appears to have little direct effect on the GP prefusion conformation.[53] The direct role of acidic pH on GP appears to be in later steps of membrane fusion: activation of the fusion loop and promotion of the six-helix bundle.[28−30]

The heptad repeat stutter at T566 is reminiscent of other stutters found in the postfusion structures of the class I viral envelope glycoproteins of EBOV GP2, lymphocytic choriomeningitis virus (LCMV) GP2, influenza virus HA2, and severe acute respiratory syndrome corona virus (SARS-CoV) S2.[42,54] It is notable that stutters are a common architectural feature among glycoproteins from these phylogenetically distinct viruses. Furthermore, stutters are also present in α-helical segments of some class III envelope glycoproteins that contain mixed α/β structure (e.g., Epstein-Barr virus gB and vesicular stomatitis virus G).[42,55,56] In long coiled-coil proteins, heptad repeat stutters are located at regular intervals.[57,58] It is believed that the translation shift in the superhelical twist (a slight unwinding) that results from the stutter stabilizes the overall fibril by preventing effects from overtwisting.[59,60] However, it is unlikely the stutters are required for this reason in the context of virus envelope glycoproteins, because the α-helical bundles are relatively short and have a larger superhelical radius because they are trimeric. In EBOV GP2 and influenza HA2, the stutters occur in regions that adopt very different structures in the prefusion and fusion-active forms. For example, the NHR segment of EBOV GP2 is interrupted into three shorter α-helices in the prefusion structure, with a major kink at the stutter position (T565).[20,21] The stutter in influenza HA2 occurs in the central stalk in a segment that adopts a loop conformation at neutral pH but a trimeric coiled coil at low pH.[23,42] Therefore, one potential role of the stutter is to provide flexibility in segments that act as a conformational switch during membrane fusion.

The sequence of MARV GP2 is 60% identical with that of EBOV GP2, and the overall structures are virtually identical, suggesting that filoviruses share a conserved mechanism for viral entry. Furthermore, the filovirus GP2 postfusion structures display a striking similarity to other fusion proteins, such as those from the evolutionarily distinct retrovirus and arenavirus families. For example, the sequence of the fusion protein from Moloney murine leukemia virus (MoMLV), a retrovirus, is <25% identical with that of filovirus GP, yet their structures display marked similarity, especially in the loop and helix−turn−helix regions. MoMLV TM is comprised of a 33-residue trimeric coiled-coil core that aligns extremely well with the filovirus GP2 α-helical core.[21,61] The available structure appears to be truncated within the coiled-coil region; however, it is predicted that the MoMLV protein core contains additional C-terminal helical residues that pack to form a trimer of hairpins, such as is seen in MARV and EBOV GP2.[22,42,60] Comparisons between filovirus GP2 and LCMV GP2 can also be drawn.[42] LCMV belongs to the arenavirus family and is known to cause severe aseptic meningitis in humans. The sequence of LCMV GP2 is <20% identical with that of filovirus GP2; again, however, the overall architectures of the fusion proteins have distinct similarities, with short CHR regions packing back into the grooves of the NHR core trimer to form a trimer of hairpins.[20,21,42] Much like MARV GP2, the postfusion state of LCMV GP2 is also stabilized by a number of salt bridges. It is interesting to note that in both cases the NHR core is elongated, with that of LCMV making 13 turns and that of MARV/EBOV making 10 turns, while the CHR regions are comparatively short, spanning only three or four turns.[20,21,42] Additionally, LCMV GP2 contains a similar loop and helix−turn−helix segments preceding the CHRs that are seen in MARV, EBOV, and MoMLV. The conservation of the glycoprotein transmembrane domain postfusion structure across these distinct viral families indicates that this configuration plays a crucial role in viral entry.

■ ASSOCIATED CONTENT

Supporting Information

Guanidine HCl denaturation of pII-MarV_{IF} and pII-MarV_{OOF}, limited proteolysis of pII-MarV_{IF} and pII-MarV_{OOF}, and mass spectrometry analysis of fragments from limited proteolysis. This material is available free of charge via the Internet at http://pubs.acs.org.

Accession Codes

The X-ray coordinates and structure factors for pII-MarV_{IF} have been deposited as Protein Data Bank entry 4G2K.

■ AUTHOR INFORMATION

Corresponding Author

*E-mail: jon.lai@einstein.yu.edu. Phone: (718) 430-8641. Fax: (718) 430-8565.

Funding

This work was funded by the Albert Einstein College of Medicine and the National Institutes of Health (NIH) (R01-AI088027, R01-AI090249, U54-GM094662, and P30-CA013330). J.S.H. was supported in part by NIH Molecular Biophysics Training Grant T32-GM008572 and J.F.K. by NIH Medical Scientist Training Grant T32-GM007288.

Notes

The authors declare no competing financial interest.

■ ACKNOWLEDGMENTS

We thank Mark Girvin for helpful discussions and members of the Lai lab for critical reading of the manuscript. We acknowledge Edward Nieves and Myrasol Callaway for performing the mass spectrometry analysis [NIH Shared Instrumentation Grant (LTQ) Mass Spectrometer System 1S10RR019352]. We thank the staff of beamline X29 at the National Synchrotron Light Source for help with data collection.

■ ABBREVIATIONS

MARV, Marburg virus; EBOV, Ebola virus; GP, glycoprotein; CatB, cathepsin B; CatL, cathepsin L; NPC1, Niemann Pick C1; NHR, N-terminal heptad repeat; CHR, C-terminal heptad repeat; PBS, phosphate-buffered saline; CD, circular dichroism; TEV, tobacco etch virus; rmsd, root-mean-square deviation.

■ REFERENCES

(1) Kuhn, J. H., Becker, S., Ebihara, H., Geisbert, T. W., Johnson, K. M., Kawaoka, Y., Lipkin, W. I., Negredo, A. I., Netesov, S. V., Nichol, S. T., Palacios, G., Peters, C. J., Tenorio, A., Volchkov, V. E., and Jahrling, P. B. (2010) Proposal for a revised taxonomy of the family Filoviridae: Classification, names of taxa and viruses, and virus abbreviations. *Arch. Virol. 155*, 2083−2103.

(2) Feldmann, H., and Geisbert, T. W. (2011) Ebola haemorrhagic fever. *Lancet 377*, 849−862.

(3) Hartman, A. L., Towner, J. S., and Nichol, S. T. (2010) Ebola and Marburg hemorrhagic fever. *Clin. Lab. Med. 30*, 161−177.

(4) Wamala, J. F., Lukwago, L., Malimbo, M., Nguku, P., Yoti, Z., Musenero, M., Amone, J., Mbabazi, W., Nanyunja, M., Zaramba, S., Opio, A., Lutwama, J. J., Talisuna, A. O., and Okware, S. I. (2010) Ebola Hemorrhagic Fever Associated with Novel Virus Strain, Uganda, 2007−2008. *Emerging Infect. Dis. 16*, 1087−1092.

(5) Lee, J. E., and Saphire, E. O. (2009) Ebolavirus glycoprotein structure and mechanism of entry. *Future Virol. 4*, 621−635.

(6) Harrison, S. C. (2008) Viral membrane fusion. *Nat. Struct. Mol. Biol. 15*, 690−698.

(7) White, J. M., Delos, S. E., Brecher, M., and Schornberg, K. (2008) Structures and mechanisms of viral membrane fusion proteins: Multiple variations on a common theme. *Crit. Rev. Biochem. Mol. Biol. 43*, 189−219.

(8) Eckert, D. M., and Kim, P. S. (2001) Mechanisms of viral membrane fusion and its inhibition. *Annu. Rev. Biochem. 70*, 777−810.

(9) Hughson, F. M. (1995) Structural characterization of viral fusion proteins. *Curr. Biol. 5*, 265−274.

(10) Lee, J. E., Fusco, M. L., Hessell, A. J., Oswald, W. B., Burton, D. R., and Saphire, E. O. (2008) Structure of the Ebola virus glycoprotein bound to an antibody from a human survivor. *Nature 454*, 177−182.

(11) Kondratowicz, A. S., Lennemann, N. J., Sinn, P. L., Davey, R. A., Hunt, C. L., Moller-Tank, S., Meyerholz, D. K., Rennert, P., Mullins, R. F., Brindley, M., Sandersfeld, L. M., Quinn, K., Weller, M., McCray, P. B., Chiorini, J., and Maury, W. (2011) T-cell immunoglobulin and mucin domain 1 (TIM-1) is a receptor for Zaire Ebolavirus and Lake Victoria Marburgvirus. *Proc. Natl. Acad. Sci. U.S.A. 108*, 8426−8431.

(12) Luczkowiak, J., Sattin, S., Sutkeviciute, I., Reina, J. J., Sanchez-Navarro, M., Thepaut, M., Martinez-Prats, L., Daghetti, A., Fieschi, F., Delgado, R., Bernardi, A., and Rojo, J. (2011) Pseudosaccharide functionalized dendrimers as potent inhibitors of DC-SIGN dependent Ebola pseudotyped viral infection. *Bioconjugate Chem. 22*, 1354−1365.

(13) Marzi, A., Akhavan, A., Simmons, G., Gramberg, T., Hofmann, H., Bates, P., Lingappa, V. R., and Pohlmann, S. (2006) The signal peptide of the ebolavirus glycoprotein influences interaction with the cellular lectins DC-SIGN and DC-SIGNR. *J. Virol. 80*, 6305−6317.

(14) Chandran, K., Sullivan, N. J., Felbor, U., Whelan, S. P., and Cunningham, J. M. (2005) Endosomal proteolysis of the Ebola virus glycoprotein is necessary for infection. *Science 308*, 1643−1645.

(15) Schornberg, K., Matsuyama, S., Kabsch, K., Delos, S., Bouton, A., and White, J. (2006) Role of endosomal cathepsins in entry mediated by the Ebola virus glycoprotein. *J. Virol. 80*, 4174−4178.

(16) Mar'iankova, R. F., Glushakova, S. E., Pyzhik, E. V., and Lukashevich, I. S. (1993) The penetration of the Marburg virus into eukaryotic cells. *Vopr. Virusol. 38*, 74−76.

(17) Carette, J. E., Raaben, M., Wong, A. C., Herbert, A. S., Obernosterer, G., Mulherkar, N., Kuehne, A. I., Kranzusch, P. J., Griffin, A. M., Ruthel, G., Dal Cin, P., Dye, J. M., Whelan, S. P., Chandran, K., and Brummelkamp, T. R. (2011) Ebola virus entry requires the cholesterol transporter Niemann-Pick C1. *Nature 477*, 340−343.

(18) Côté, M., Misasi, J., Ren, T., Bruchez, A., Lee, K., Filone, C. M., Hensley, L., Li, Q., Ory, D., Chandran, K., and Cunningham, J. (2011) Small molecule inhibitors reveal Niemann-Pick C1 is essential for Ebola virus infection. *Nature 477*, 344−348.

(19) Misasi, J., Chandran, K., Yang, J. Y., Considine, B., Filone, C. M., Cote, M., Sullivan, N., Fabozzi, G., Hensley, L., and Cunningham, J. (2012) Filoviruses require endosomal cysteine proteases for entry but exhibit distinct protease preferences. *J. Virol. 86*, 3284−3292.

(20) Weissenhorn, W., Carfi, A., Lee, K. H., Skehel, J. J., and Wiley, D. C. (1998) Crystal structure of the Ebola virus membrane fusion subunit, GP2, from the envelope glycoprotein ectodomain. *Mol. Cell 2*, 605−616.

(21) Malashkevich, V. N., Schneider, B. J., McNally, M. L., Milhollen, M. A., Pang, J. X., and Kim, P. S. (1999) Core structure of the envelope glycoprotein GP2 from Ebola virus at 1.9-Å resolution. *Proc. Natl. Acad. Sci. U.S.A. 96*, 2662−2667.

(22) Carr, C. M., and Kim, P. S. (1993) A spring-loaded mechanism for the conformational change of influenza hemagglutinin. *Cell 73*, 823−832.

(23) Bullough, P. A., Hughson, F. M., Skehel, J. J., and Wiley, D. C. (1994) Structure of the influenza haemaglutinin at the pH of membrane fusion. *Nature 371*, 37−43.

(24) Qin, Z., Zheng, Y., and Kielian, M. (2009) Role of Conserved Histidine Residues in the Low-pH Dependence of the Semliki Forest Virus Fusion Protein. *J. Virol. 83*, 4670−4677.

(25) Liu, C. Y., and Kielian, M. (2009) E1 mutants identify a critical region in the trimer interface of the Semliki forest virus fusion protein. *J. Virol. 83*, 11298−11306.

(26) Sanchez-San Martin, C., Liu, C. Y., and Kielian, M. (2009) Dealing with low pH: Entry and exit of alphaviruses and flaviviruses. *Trends Microbiol. 17*, 514−521.
(27) Harrison, S. C. (2008) The pH sensor for flavivirus membrane fusion. *J. Cell Biol. 183*, 177−179.
(28) Gregory, S. M., Harada, E., Liang, B., Delos, S. E., White, J. M., and Tamm, L. K. (2011) Structure and function of the complete internal fusion loop from Ebolavirus glycoprotein 2. *Proc. Natl. Acad. Sci. U.S.A. 108*, 11211−11216.
(29) Harrison, J. S., Higgins, C. D., Chandran, K., and Lai, J. R. (2011) Designed protein mimics of the Ebola virus glycoprotein GP2 α-helical bundle: Stability and pH effects. *Protein Sci. 20*, 1587−1596.
(30) Harrison, J. S., Koellhoffer, J. F., Chandran, K., and Lai, J. R. (2012) Marburg virus glycoprotein GP2: pH-dependent stability of the ectodomain α-helical bundle. *Biochemistry 51*, 2515−2525.
(31) Otwinowski, Z. M., and Minor, W. (1997) Processing of X-ray Diffraction Data Collected in Oscillation Mode. *Methods Enzymol. 276*, 307−326.
(32) Collaborative Computational Project, Number 4 (1994) The CCP4 Suite: Programs for Protein Crystallography. *Acta Crystallogr. 50*, 760−763.
(33) Storoni, L. C., McCoy, A. J., and Read, R. J. (2004) Likelihood-enhanced fast rotation functions. *Acta Crystallogr. D60*, 432−438.
(34) Emsley, P., and Cowtan, K. (2004) Coot: Model-building tools for molecular graphics. *Acta Crystallogr. D60*, 2126−2132.
(35) Chen, B. V., Arendall, W. B., Headd, J. J., Keedy, D. A., Immormino, R. M., Kapral, G. J., Murray, L. W., Richardson, J. S., and Richardson, D. C. (2010) MolProbity: All-atom structure validation for macromolecular crystallography. *Acta Crystallogr. D66*, 12−21.
(36) Krissinel, E., and Henrick, K. (2004) Secondary-structure matching (SSM), a new tool for fast protein structure alignment in three dimensions. *Acta Crystallogr. D60*, 2256−2268.
(37) Harbury, P. B., Kim, P. S., and Alber, T. (1994) Crystal structure of an isoleucine-zipper trimer. *Nature 371*, 80−83.
(38) Weissenhorn, W., Dessen, A., Harrison, S. C., Skehel, J. J., and Wiley, D. C. (1997) Atomic structure of the ectodomain from HIV-1 gp41. *Nature 387*, 426−430.
(39) Tan, K., Liu, J., Wang, J., Shen, S., and Lu, M. (1997) Atomic structure of a thermostable subdomain of HIV-1 gp41. *Proc. Natl. Acad. Sci. U.S.A. 94*, 12303−12308.
(40) Occhionorelli, M., Santoro, F., Pallavicini, I., Gruszka, A., Moretti, S., Bossi, D., Viale, A., Shing, D., Ronzoni, S., Muradore, I., Soncini, M., Pruneri, G., Rafaniello, P., Viale, G., Pelicci, P. G., and Minucci, S. (2011) The self-association coiled-coil domain of PML is sufficient for the oncogenic conversion of the retinoic acid receptor (RAR) α. *Leukemia 25*, 814−820.
(41) Weissenhorn, W., Calder, L. J., Dessen, A., Laue, T., Skehel, J. J., and Wiley, D. C. (1997) Assembly of a rod-shaped chimera of a trimeric GCN4 zipper and the HIV-1 gp41 ectodomain expressed in *Escherichia coli*. *Proc. Natl. Acad. Sci. U.S.A. 94*, 6065−6069.
(42) Igonet, S., Vaney, M. C., Vonhrein, C., Bricogne, G., Stura, E. A., Hengartner, H., Eschli, B., and Rey, F. A. (2011) X-ray structure of the arenavirus glycoprotein GP2 in its postfusion hairpin conformation. *Proc. Natl. Acad. Sci. U.S.A. 108*, 19967−19972.
(43) Oakley, M. G., and Kim, P. S. (1998) A Buried Polar Interaction Can Direct the Relative Orientation of Helices in a Coiled Coil. *Biochemistry 37*, 12603−12610.
(44) McClain, D. L., Binfet, J. P., and Oakley, M. G. (2001) Evaluation of the Energetic Contribution of Interhelical Coulombic Interactions for Coiled Coil Helix Orientation Specificity. *J. Mol. Biol. 313*, 371−383.
(45) Akey, D. L., Malashkevich, V. N., and Kim, P. S. (2001) Buried Polar Residues in Coiled-Coil Interfaces. *Biochemistry 40*, 6352−6360.
(46) O'Shea, E. K., Lumb, K. J., and Kim, P. S. (1993) Peptide 'Velcro': Design of a heterodimeric coiled coil. *Curr. Biol. 3*, 658−667.
(47) Lumb, K. J., and Kim, P. S. (1995) A Buried Polar Interaction Imparts Structural Uniqueness in a Designed Heterodimeric Coiled Coil. *Biochemistry 34*, 8642−8648.
(48) O'Shea, E. K., Rutkowski, R., Stafford., W. F., and Kim, P. S. (1989) Preferential Heterodimer Formation by Isolated Leucine Zippers from Fos and Jun. *Science 245*, 646−648.
(49) Lau, W. L., Degrado, W. F., and Roder, H. (2010) The Effects of pKa Tuning on the Thermodynamics and Kinetics of Folding: Design of a Solvent-Shielded Carboxylate Pair at the a-Position of a Coiled-Coil. *Biophys. J. 99*, 2299−2308.
(50) Marti, D. N., and Bosshard, H. R. (2003) Electrostatic interactions in leucine zippers: Thermodynamic analysis of the contributions of Glu and His residues and the effect of mutating salt bridges. *J. Mol. Biol. 330*, 621−637.
(51) Markley, J. L., and Song, S. (2007) Cautionary Tail: The Presence of an N-Terminal Tag on Dynein Light-Chain Roadblack/LC7 Affects Its Interaction with a Functional Partner. *Protein Pept. Lett. 14*, 265−268.
(52) Lumb, K. J., and Kim, P. S. (1995) Measurement of Interhelical Electrostatic Interactions in the GCN4 Leucine Zipper. *Science 268*, 436−439.
(53) Bale, S., Liu, T., Li, S., Wang, Y., Abelson, D., Fusco, M., Woods, V. L., and Saphire, E. O. (2011) Ebola Virus Glycoprotein Needs an Additional Trigger, beyond Proteolytic Priming for Membrane Fusion. *PLoS Neglected Trop. Dis. 5*, e1395.
(54) Supekar, V. M., Bruckmann, C., Ingallinella, P., Bianchi, E., Pessi, A., and Carfi, A. (2004) Structure of a proteolytically resistant core from the severe acute respiratory syndrome coronavirus S2 fusion protein. *Proc. Natl. Acad. Sci. U.S.A. 101*, 17958−17963.
(55) Backovic, M., Longnecker, R., and Jardetzky, T. S. (2009) Structure of a trimeric variant of the Epstein-Barr virus glycoprotein B. *Proc. Natl. Acad. Sci. U.S.A. 106*, 2880−2885.
(56) Roche, S., Bressanelli, S., Rey, F. A., and Gaudin, Y. (2006) Crystal structure of the low-pH form of the vesicular stomatits virus glycoprotein. *Science 313*, 187−191.
(57) Lu, S. M., and Hodges, R. S. (2004) Defining the minimum size of a hydrophobic cluster in two-stranded α-helical coiled-coils: Effects on protein stability. *Protein Sci. 13*, 714−726.
(58) Lupas, A. N., and Gruber, M. (2005) The structure of α-helical coiled coils. *Adv. Protein Chem. 70*, 37−78.
(59) Strelkov, S. V., and Burkhard, P. (2002) Analysis of α-Helical Coiled Coils with the Program TWISTER Reveals a Structural Mechanism for Stutter Compensation. *J. Struct. Biol. 137*, 54−64.
(60) Brown, J. D., Cohen, C., and Parry, D. A. (1996) Heptad breaks in α-helical coiled coils: Stutters and stammers. *Proteins 26*, 134−145.
(61) Fass, D., Harrison, S. C., and Kim, P. S. (1996) Retrovirus envelope domain at 1.7 angstrom resolution. *Nat. Struct. Biol. 3*, 465−469.
(62) Jo, S., Vargyas, M., Vasko-Szedlar, J., Roux, B., and Im, W. (2008) PBEQ-Solver for online visualization of electrostatic potential of biomolecules. *Nucleic Acids Res. 36*, 270−275.
(63) Im, W., Beglov, D., and Roux, B. (1998) Continuum Solvation Model: Computation of Electrostatic Forces from Numerical Solutions to the Poisson-Boltzmann Equation. *Comput. Phys. Commun. 111*, 59−75.
(64) Brooks, B. R., Bruccoleri, R. E., Olafson, B. D., States, D. J., Swaminathan, S., and Karplus, M. (1983) CHARMM: A program for macromolecular energy minimization and dynamics calculations. *J. Comput. Chem. 4*, 187−217.